

Measurement of ablation threshold of oxide-film-coated aluminium nanoparticles irradiated by femtosecond laser pulses

O.V. Chefonov, A.V. Ovchinnikov, I.V. Il'ina, M.B. Agranat

Abstract. We report the results of experiments on estimation of femtosecond laser threshold intensity at which nanoparticles are removed from the substrate surface. The studies are performed with nanoparticles obtained by femtosecond laser ablation of pure aluminium in distilled water. The attenuation (or extinction, i.e. absorption and scattering) spectra of nanoparticles are measured at room temperature in the UV and optical wavelength ranges. The size of nanoparticles is determined using atomic force microscopy. A new method of scanning photoluminescence is proposed to evaluate the threshold of nanoparticle removal from the surface of a glass substrate exposed to IR femtosecond laser pulses with intensities 10^{11} – 10^{13} W cm⁻².

Keywords: femtosecond laser pulse, luminescence, nanoparticles.

1. Introduction

Micro- and nanostructuring of aluminium [1–3] and preparation of aluminium nanoparticles and nanoclusters are not only of scientific but also of practical interest. Aluminium is the cheapest of plasmon materials (gold, silver, etc.) and has a relatively low melting point, which greatly simplifies synthesis of nanoparticles [2]. At the same time, the range of possible applications of aluminium nanoparticles is continuously expanding: Due to their optical characteristics they can be used in plasmonics [4–6] and optoelectronics (as power attenuators [2], in metal-enhanced fluorescence to detect biomolecules [7, 8], and in surface-enhanced Raman spectroscopy [9]), as well as in improved fuel mixtures [10] (in particular, rocket propellants [11]), because they have an increased heat transfer (in the case of exothermic oxidation reaction) and ignition probability [11].

Among many currently developed methods of fabrication of aluminium nanoparticles and nanoclusters [2, 5, 12], laser ablation has a number of significant advantages [12] because it allows synthesis of nanoparticles with different sizes and structure (including hollow ones [13, 14]), as well as high purity and narrow size distribution. In laser ablation of aluminium use is often made of nanosecond [15], picosecond [16] and femtosecond [2, 16–18] lasers. The latter have an advantage because they make it possible to minimise oxidation of

the surface of nanoparticles [13, 16] by reducing the time of interaction of aluminium with the surrounding liquid.

The morphology obtained by laser ablation of nanoparticles and the degree of oxidation depend not only on laser parameters (wavelength, pulse duration, intensity), but also on the type of the solution used (despite the fact that laser ablation of aluminium is also possible in vacuum and air, collection of nanoparticles synthesised in liquids is more convenient). For laser ablation and fabrication of aluminium nanoparticles and nanoclusters use is made of the following solvents: water [15, 16]; ethanol [16, 19], acetone and ethylene glycol [19]; polar and nonpolar organic solvents such as chloroform and carbon tetrachloride, respectively [20]; and non-ionic polymers and anionic surfactants [21]. Using ethanol instead of acetone favours the formation of smaller nanoparticles with a narrow size distribution [21]. The presence of a gas dissolved in a liquid also affects the structure of synthesised nanoparticles [13]. Thus, saturation of a liquid with hydrogen leads to the formation of cavities in nanoparticles [14]. Preparation of aluminium oxide (Al₂O₃) nanoparticles is also of practical interest in view of the properties of the latter, namely, high stability, strength, transparency and very effective insulation properties.

In this paper we present the results of experiments aimed at determining the laser intensity at which nanoparticles produced by femtosecond laser ablation of aluminium in distilled water are removed from the surface of a glass substrate irradiated by IR femtosecond laser pulses. A new original method of femtosecond scanning photoluminescence is proposed and implemented for diagnostics of the presence of nanoparticles on the substrate surface.

2. Synthesis of nanoparticles

Nanoparticles were synthesised by femtosecond laser ablation of pure aluminium immersed in distilled water. This method allows one to obtain chemically pure nanoparticles that are free of surfactants and can be used in further studies without additional preparation and treatment (as opposed to commonly used methods of chemical synthesis).

Aluminium nanoparticles produced in laser ablation of pure aluminium in distilled water are transformed in an aqueous solution either into aluminium oxide nanoparticles or aluminium nanoparticles coated by a thin aluminium oxide layer as a result of interaction with oxygen. The degree of oxidation of aluminium nanoparticles depends on the pulse duration and laser wavelength. In using femtosecond laser pulses, the thickness of the oxide layer formed on the surface of an aluminium nanoparticle does not exceed the thickness of the oxide film resulting from natural oxidation of aluminium

O.V. Chefonov, A.V. Ovchinnikov, I.V. Il'ina, M.B. Agranat Joint Institute for High Temperatures, Russian Academy of Sciences, ul. Izhorskaya 13, Bld. 2, 125412 Moscow, Russia; e-mail: ovtch2006@yandex.ru

Received 13 November 2015; revision received 25 January 2016
Kvantovaya Elektronika 46 (3) 223–228 (2016)
Translated by I.A. Ulitkin

and prevents further formation of the oxide film. Laser UV radiation with a wavelength close to that of the plasmon resonance of synthesised nanoparticles can cause additional heating, which leads to a more effective interaction with the environment containing nanoparticles and, consequently, to their complete oxidation [16, 22].

Thus, metal aluminium nanoparticles should be synthesised in oxygen-free liquids exposed to femtosecond laser pulses at a wavelength that is different from that of the plasmon resonance of the nanoparticles produced.

As a source of laser pulses we used a femtosecond laser system with an active medium based on a tungstate crystal doped with ytterbium (Yb:KYW) (TETA laser system, Avesta-Project). The femtosecond laser allowed the generation of laser pulses with a duration of 285 fs at a wavelength $\lambda = 1028$ nm, which were then converted using a nonlinear optical crystal into pulses with a wavelength $\lambda = 514$ nm (second harmonic) and a maximum energy of 6 mJ. The laser pulse repetition rate was 5 kHz.

Laser radiation was focused onto the target by a LOMO $10\times$ microlens with a numerical aperture $NA = 0.25$. The focal spot size of laser radiation on the target was determined by the method from [23], according to which we first plotted the dependence of the square radius of the ablation crater of a silicon array on the logarithm of the energy of a single laser pulse, and then using the linear approximation of experimental points we determined the Gaussian beam parameter r_0 . For $\lambda = 514$ nm, the transverse size of the focal spot was $2.2 \mu\text{m}$ at the $1/e$ of the maximum intensity, and the threshold energy density at which silicon is ablated was equal to $0.52 \pm 0.06 \text{ J cm}^{-2}$.

As a target for synthesis of nanoparticles we used a polished plane-parallel high-purity aluminium (grade A999) plate of thickness $500 \mu\text{m}$ and area of 1 cm^2 . The target was placed in a Petri dish which was filled with 5 mL of distilled water. Laser radiation was launched through a $170\text{-}\mu\text{m}$ -thick quartz glass glued into the bottom of the Petri dish. The thickness of the liquid layer between the glass and the target was 2 mm. The Petri dish with the target was placed onto a software-controlled motorised XY sample stage of an inverted microscope. The stage was continuously moved along a predetermined trajectory during the laser pulse action on the target. Nanoparticles were synthesised at an energy density (32 J cm^{-2}) of laser radiation incident on the surface of the aluminium target. The synthesis time was 2.5 h.

For further investigation and reduction of the nanoparticle size dispersion, the initial aqueous solution containing large ablation products of the aluminium target and nanoparticles was subjected to two-step centrifugation with a centrifuge speed of 3000 rpm. The duration of the centrifugation step was 20 min.

3. Extinction spectra of nanoparticles

To study the optical and plasmonic properties of the synthesised nanoparticles, we measured extinction spectra of nanoparticles located in a distilled water solution in the UV and visible wavelength ranges. Using a SF-26 spectrophotometer we first determined the transmittance T of the nanoparticles, equal to the ratio of the intensity I of the radiation flux passing through the cell with a nanoparticle solution in distilled water to the intensity I_0 of the radiation flux passing through the cell with nanoparticle-free distilled water. Then, we plotted

the wavelength dependence of the value of extinction $1 - T$. Figure 1 shows the extinction spectra of the synthesised aluminium nanoparticles before and after centrifugation. One can see that after this procedure the extinction spectrum of the nanoparticles becomes narrower in comparison with the initial spectrum and the long-wavelength part of the spectrum (450–800 nm) is blueshifted (300–450 nm). In this case, the maximum in the extinction spectrum at $\lambda = 200$ nm becomes pronounced and a spectral feature in the vicinity of $\lambda = 250$ nm begins to emerge.

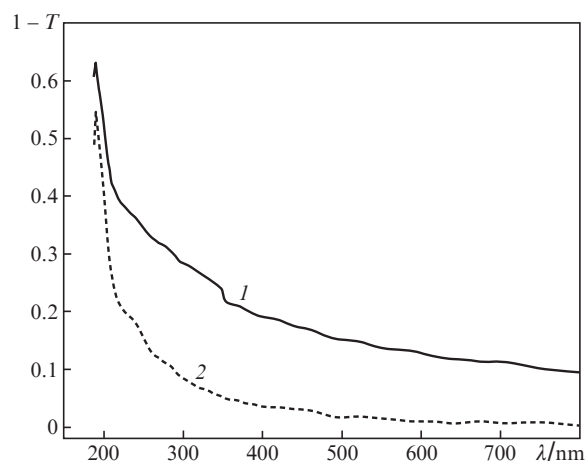


Figure 1. Experimental extinction spectra of aluminium nanoparticles before (1) and after (2) centrifugation.

As shown by theoretical calculations of the absorption spectra of an aqueous solution of spherical aluminium nanoparticles [24], the plasmon resonance peak for particles with a diameter of 10 nm corresponds to ~ 200 nm, and its red shift is explained by an increase in the transverse size of the nanoparticles [6, 24, 25]. On the other hand, the red shift of the plasmon resonance of aluminium nanoparticles can be caused by their oxidation, because in the UV wavelength range the refractive index of aluminium oxide is greater than that of water. Thus, for an aqueous solution of 20–50 nm aluminium oxide nanoparticles the maximum of the absorption spectrum corresponds to $\lambda = 210$ nm [26]. Typically, the thickness of the aluminium oxide layer on the nanoparticle is 1.7–6.0 nm and is independent of its size [27].

Thus, based on the measurements of the extinction spectra and on the analysis of previously performed experiments, we can assume that in the process of femtosecond laser ablation of aluminium in distilled water we synthesised aluminium nanoparticles coated with a thin layer of an oxide film.

4. Evaluation of the size of the nanoparticles

Figure 2 shows a three-dimensional image of the surface topography of the substrate with the deposited nanoparticles. The image was obtained using an atomic force microscope (AFM) by a semi-contact method for studying surfaces. The sample was prepared by drying a droplet of an aqueous solution of aluminium nanoparticles on a mica substrate.

Figure 3 shows AFM images of the surface topography of the substrate with the nanoparticles and the surface cross-sectional profiles constructed along the respective lines.

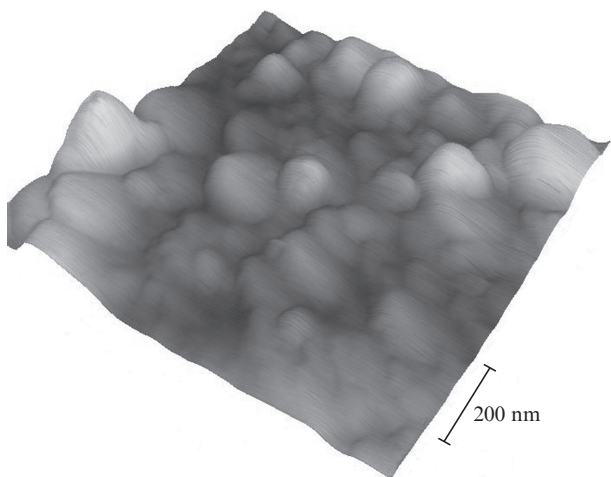


Figure 2. Three-dimensional AFM image of the substrate surface with the nanoparticles.

Despite the fact that the atomic force microscopy allows a high spatial resolution, the data on the relief of the surface under study do not always adequately reflect the real features of the surface. This is primarily due to the fact that the AFM images are completely different (in physics of processes underlying imaging) from images formed using a conventional optical microscope or an electron microscope, which exclude the impact of the research tool on an object and produce no image artifacts. In fact, there exist the following sources of artifacts of AFM images: probe tip of a cantilever, nonlinearity of the positioner (scanner) movement, external vibration, noise in the feedback loop and errors in software image processing. The most common artifacts of atomic force microscopy are those associated with the probe: the effect of ‘profile broadening’ due to the convolution of the probe shape with the shape of the object (the probe size is greater than or comparable to the size of the object), and the effect of ‘height flattening’ due to the elastic deformation of the objects in question.

In our measurements we used a semi-contact (tapping) scanning method according to which the probe tip periodi-

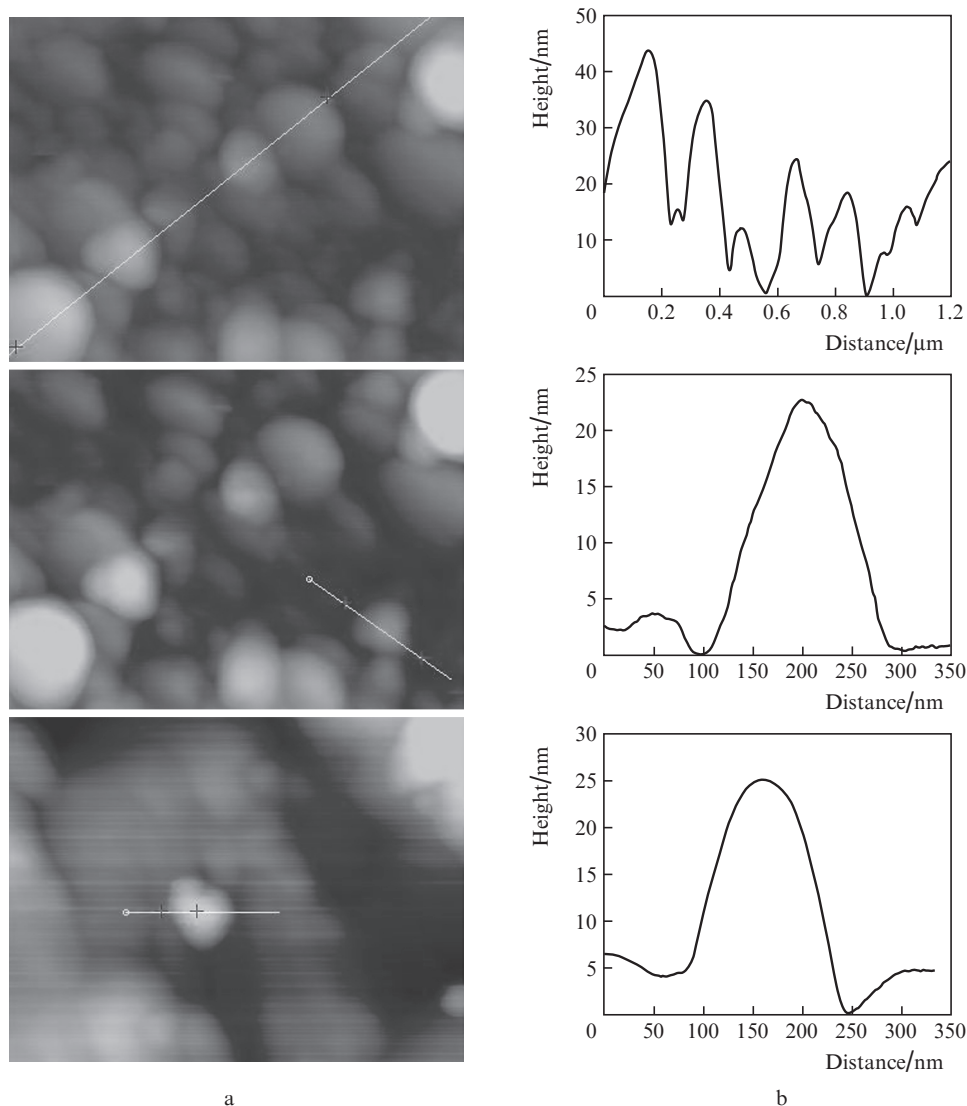


Figure 3. (a) AFM images of the surface topography of the substrate with the nanoparticles and (b) surface cross-sectional profiles constructed along the respective lines in Fig. 3a.

cally touches the sample surface under oscillation, but only for a small part of the oscillation period. This method is widely used in studies of nanostructured surfaces and has certain advantages over contact methods. First of all, in this method the probe tip produces less pressure on the surface, which makes it appropriate for fragile and soft samples. The main artifact of the semi-contact method is the effect of 'profile broadening', i.e. the transverse size of protruding objects on the sample surface is much greater than the real size, and its value can only be used as the upper limit for the true size estimates. However, the height of the objects will be determined fairly accurately. In analysing the data presented in Fig. 3, it can be concluded that the diameter of the synthesised nanoparticles is about 10–45 nm.

5. Measurement of the removal threshold of nanoparticles from the substrate surface

To measure the threshold intensity of a femtosecond laser pulse, at which synthesised nanoparticles are removed from the surface of a glass substrate, we proposed and implemented a femtosecond photoluminescence scanning method.

The method consists in a sequential measurement of the spectrum- and time-integrated intensity of photoluminescence of nanoparticles in the same region on the substrate and in the same wavelength range before and after the action of a heating laser pulse, as well as in a subsequent analysis of the relationship of integrated photoluminescence intensity before and after exposure as a function of the energy density of the heating laser pulse or its intensity.

Single-, two- and multiphoton luminescence of bulks and nanoparticles of d-block metals that occurs under their irradiation by nano- and femtosecond laser pulses is well known [23, 28–30]. The authors of Refs [31–33] studied single-photon excitation of luminescence of aluminium oxide by UV radiation. In the case of oxide-film-coated aluminium nanoparticles exposed to IR femtosecond laser pulses, multiphoton absorption in the aluminium oxide layer results in luminescence excitation, which is a kind of a marker that determines the presence of a nanoparticle.

Photoluminescence of nanoparticles was excited due to multiphoton absorption of IR radiation of a TEMA laser (Avesta Project) at $\lambda = 1048$ nm with a pulse duration of 110 fs, a pulse energy of about 3 nJ, and a pulse repetition rate of 71 MHz [28, 29]. The energy of the probing femtosecond laser pulse was chosen sufficient to firstly ensure the maximum photoluminescence quantum yield of nanoparticles without damaging the region with the nanoparticles on the substrate, and secondly to ensure the absence photoluminescence under irradiation of a clean substrate without nanoparticles by a laser pulse. The laser beam was focused onto the sample by a LOMO 20 \times microlens with a numerical aperture $NA = 0.4$ to a spot with a diameter of ~ 2 μm . The maximum energy density at the sample was 60 mJ cm^{-2} in view of the transmittance of the optical elements of the optical scheme.

Emission of photoluminescence collected by a microlens was directed onto the entrance slit of an Acton SP2300i spectrograph. The spectrograph employed a ruled diffraction grating (50 lines mm^{-1} , Richardson gratings) with a maximum of reflection efficiency at $\lambda = 600$ nm. Using a grating with a small number of lines made it possible to record spectra in the 400–650 nm range per measurement. The boundaries of the spectral range were determined by the detector sensitivity in

the red region of the spectrum and the diffraction grating efficiency in the blue region. As a radiation detector we used an intensified high-sensitivity cooled CCD camera (PI-MAX). In the spectrometric path between the microlens and the spectrograph slit we installed a bandpass filter that protected the CCD camera from the laser light at $\lambda = 1048$ nm. The exposure time of one frame of the CCD camera was 25 ms. The signal accumulation was carried out by the summation of 40 exposures.

Two-dimensional images of the spectra were summed up along the spatial coordinate in the wavelength range of 500–650 nm. The bandwidth (along the spatial coordinate) was chosen slightly larger than the photoluminescence spot.

The sample in question was prepared as follows. A drop of an aqueous solution of aluminium nanoparticles with a volume of 10 μL was first placed on a 170- μm -thick sterile plane-parallel glass plate and then dried in a FASTER TWO-30 laminar flow cabinet in a dust-free air environment.

As a source of heating laser pulses we used a TETA femtosecond laser system (Avesta Project), which generated single laser pulses. For this purpose, the experimental scheme employed a pulse selector consisting of an electro-optic modulator mounted between two crossed Glan–Thompson prisms, a high-voltage generator, a time delay unit and a control unit. A polarisation attenuator, which consisted of a half-wave plate and a Glan–Thompson prism, allowed the laser pulse energy to be tuned from a few nanojoules to a few microjoules. The laser pulse energy measurements were performed using a calorimeter and a calibrated photodiode with a set of neutral filters.

The heating laser beam was focused onto the sample by the same microlens, as was the case of photoluminescence excitation; however, the size of the heating laser pulse spot was four times larger than the spot size of the laser light exciting the luminescence. This was done in order to ensure a guaranteed penetration of the probe laser pulse in the area of the heating laser pulse action. To change the size of the laser spot on the sample we used a telescope, assembled in accordance with a Galilean scheme, which changed the divergence of the laser radiation. The diameter of the heating laser beam spot in the sample plane was ~ 8 μm .

Each new pair of spectra (before and after the heating pulse action) at a specific energy density of a laser pulse was measured at a new location on the sample. In the experiments, the maximum energy of the heating laser pulse was limited by the energy at which the glass substrate with nanoparticles began to degrade.

The removal threshold of the nanoparticles, which were deposited on a glass substrate subjected to IR femtosecond laser pulses, in the air was studied for three different heating laser pulse durations of 270, 540 and 750 fs in the same range of energies. Figures 4 and 5 show the ratio of the luminescence intensity I_{fin} of the nanoparticles after the exposure to the heating laser pulse to the luminescence intensity I_{in} before the exposure as a function of the intensity and energy density of the heating laser pulse at its different durations.

One can see from Fig. 4 that all the experimental points lie on the same curve at different durations of the heating laser pulse. A decrease in the yield of multiphoton photoluminescence of nanoparticles is associated with a change in their number in the interaction region and occurs with the same intensity and different pulse durations. An insignificant photoluminescence level at intensities higher than 1.5×10^{13} W cm^{-2}

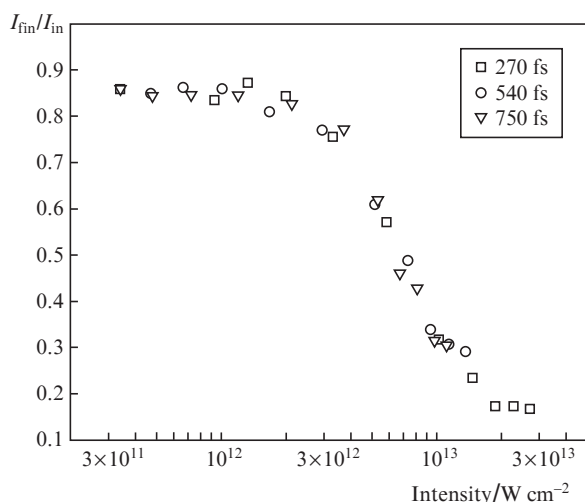


Figure 4. Ratio I_{fin}/I_{in} of the nanoparticle luminescence intensities before and after the heating laser pulse action as a function of the intensity of this pulse at its different durations.

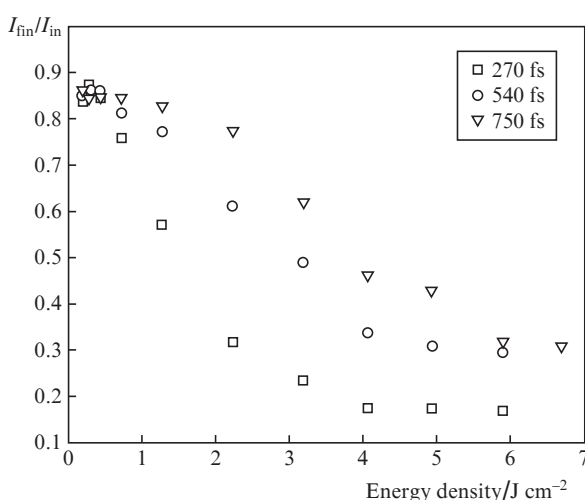


Figure 5. Ratio I_{fin}/I_{in} of the nanoparticle luminescence intensities before and after the heating laser pulse action as a function of the energy density of this pulse at its different durations.

is possibly due to the fact that the modified surface of the substrate is doped by a small number of nanoparticles. At heating pulse intensities less than 10^{12} W cm^{-2} , one observes a slight reduction in the yield of luminescence, which results from the modification of nanoparticles and from changes in their spatial distribution in the region of the heating laser pulse action [23].

6. Conclusions

We have used the method of femtosecond laser ablation of the surface of pure aluminium in distilled water to synthesise 10–45 nm (using AFM) nanoparticles. We have measured the transmission spectrum of an aqueous solution with nanoparticles. A new method of femtosecond scanning multiphoton photoluminescence has been employed to obtain new data on the IR femtosecond laser pulse intensity ($\sim 10^{12}$ W cm^{-2})

at which nanoparticles deposited on a glass substrate are removed. The dependence of the energy density of a laser pulse on its duration in the range of 100–1000 fs has been studied. Analysis of the experimental results shows that the removal of the nanoparticles is completely governed by the femtosecond laser pulse intensity.

Acknowledgements. All experimental studies have been performed using a combined ‘femtosecond laser scalpel–optical tweezers’ system and equipment developed at the Joint Institute for High Temperatures (JIHT) of the Russian Academy of Sciences (RAS) and used as part of the Centre for Collective Use ‘Laser Femtosecond Complex’ at the JIHT RAS.

This work was supported by the Russian Science Foundation (Project No. 14-19-01487).

References

1. Perrie W., Gill M., Robinson G., Fox P., O'Neill W. *Appl. Surf. Sci.*, **230**, 50 (2004).
2. Kuladeep R., Dar M.H., Deepak K.L.N., Rao D.N. *J. Appl. Phys.*, **116**, 113107 (2014).
3. Stratakis E., Zorba V., Barberoglou M., Fotakis C., Shafeev G.A. *Appl. Surf. Sci.*, **255**, 5346 (2009).
4. Katyal J., Soni R.K. *J. Mod. Opt.*, **60**, 1717 (2013).
5. Martin J., Plain J. *J. Phys. D: Appl. Phys.*, **48**, 184002 (2015).
6. Ekinci Y., Solak H., Löffler J. *J. Appl. Phys.*, **104**, 083107 (2008).
7. Chowdhury M.H., Ray K., Gray S.K., Pond J., Lakowicz J.R. *Anal. Chem.*, **81**, 1397 (2009).
8. Kabashin A.V., Evans P., Pastkovsky S., Hendren W., Wurtz G.A., Atkinson R., Pollard R.J., Podolskiy V.A., Zayats A.V. *Nat. Mater.*, **8**, 867 (2009).
9. Zhou X., Fang Y., Zhang P. *Spectrochim. Acta, Part A*, **67**, 122 (2007).
10. Tyagi H., Phelan P.E., Prasher R., Peck R., Lee T., Pacheco J.R., Arentzen P. *Nano Lett.*, **8**, 1410 (2008).
11. Galfetti L., De Luca L.T., Severini F., Meda L., Marra G., Marchetti M., Regi M., Bellucci S. *J. Phys.: Condens. Matter*, **18**, S1991 (2006).
12. Ghorbani H.R. *Orient. J. Chem.*, **30**, 1941 (2014).
13. Viau G., Colliere V., Lacroix L.-M., Shafeev G.A. *Chem. Phys. Lett.*, **501**, 419 (2011).
14. Kuzmin P.G., Shafeev G.A., Viau G., Warot-Fonrose B., Barberoglou M., Stratakis E., Fotakis C. *Appl. Surf. Sci.*, **258**, 9283 (2012).
15. Kumar B., Thareja R.K. *J. Appl. Phys.*, **108**, 064906 (2010).
16. Stratakis E., Zorba V., Barberoglou M., Fotakis C., Shafeev G.A. *Nanotechnology*, **20**, 105303 (2009).
17. Podagatlapalli G.K., Hamad S., Sreedhar S., Tewari S.P., Rao S.V., *Chem. Phys. Lett.*, **530**, 93 (2012).
18. Stratakis E., Barberoglou M., Fotakis C., Viau G., Garcia C., Shafeev G.A. *Opt. Express*, **17**, 12650 (2009).
19. Baladi A., Mamooory R.S. *Appl. Surf. Sci.*, **256**, 7559 (2010).
20. Kuladeep R., Jyothi L., Prakash P., Shekhar S.M., Prasad M.D., Rao D.N. *J. Appl. Phys.*, **114**, 243101 (2013).
21. Singh R., Soni R.K. *Appl. Phys. A*, **116**, 689 (2014).
22. Hornyak G.L., Phani K.L.N., Kunked D.L., Menon V.P., Martin C.R. *Nanostruct. Mater.*, **6**, 839 (1995).
23. Chefonov O.V., Sitnikov D.S., Ilna I.V., Kotelev M.S., Novikov A.A., Ovchinnikov A.V. *High Temp.*, **53**, 605 (2015).
24. Creighton J.A., Eadon D.G. *J. Chem. Soc., Faraday Trans.*, **87**, 3881 (1991).
25. Martin J., Proust J., Gerard D., Plain J. *Opt. Mater. Express*, **3**, 954 (2013).
26. Piriyaawong V., Thongpool V., Asanithi P., Limsuwan P. *J. Nanomater.* Doi:10.1155/2012/819403.
27. Pesiri D., Aumann C.E., Bilger L., Booth D., Carpenter R.D., Dye R., O'Neill E., Shelton D., Walter K.C. *J. Pyrotech.*, **19**, 19 (2004).

28. Agranat M.B., Anisimov S.I., Ashitkov S.I., Chefonov O.V., Ovchinnikov A.V., Perelman L.T., Sitnikov D.S., Yurkevich A.A., Fortov V.E. *Pis'ma Zh. Eksp. Teor. Fiz.*, **101**, 671 (2015).
29. Sitnikov D.S., Yurkevich A.A., Kotelev M.S., Ziangirova M., Chefonov O.V., Ilina I.V., Vinokurov V.A., Muradov A.V., Itzkan I., Agranat M.B., Perelman L.T. *Laser Phys. Lett.*, **11**, 075902 (2014).
30. Boyd G.T., Yu Z.H., Shen Y.R. *Phys. Rev. B*, **33**, 7923 (1986).
31. Komarov F.F., Mudryi A.V., Vlasukova L.A., Mukhurov N.I., Ivanyukovich A.V. *Opt. Spektrosk.*, **104**, 272 (2008).
32. Kortov V.S., Ermakov A.E., Zatsepin A.F., Uimin M.A., Nikiforov S.V., Mysik A.A., Gaviko V.S. *Fiz. Tverd. Tela*, **50**, 916 (2008).
33. Sufeng Liu, Ligong Zhang, Yi Fan, Jinsong Luo. *App. Phys. Lett.*, **89**, 051911 (2006).